ACS OMEGA

Open Access

http://pubs.acs.org/journal/acsodf

Article

Effect of PAM on Surface Hydrophobicity of Montmorillonite and Difference of Interface Adsorption: An Experimental and Simulation Study

Xiaohui Yan, Qi Meng, Mohamed-Tahar Ammami,* and Lubin Wei*

Cite This: *ACS Omega* 2024, 9, 15818−15832

Read Online

ACCESS | Metrics & More | Article Recommendations | Supporting Information

ABSTRACT: How to realize efficient treatment of coal slime generated by a coal washing operation is an urgent problem to be solved in this industry. The presence of clay minerals, especially highly hydrophilic montmorillonite (MMT), is the key to the poor treatment effect of coal slime. Polyacrylamide (PAM) is very popular as a polymer agent to improve the treatment of coal slime. However, when it is used to treat coal slime with a high content of MMT, the selection of PAM type and the mechanism of action are still lacking. In this study, the effects of different types of PAM on the treatment of coal slime water containing MMT are considered by sedimentation and press filtration tests. The interaction mechanism of PAM on the MMT surface is studied by using ζ-potential, Brunauer−Emmett−Teller (BET) analysis, low-field nuclear magnetic resonance, density functional theory (DFT), and molecular dynamics (MD) simulations. The results show that the three PAM can improve the sedimentation and filtration effect of coal slime water, and the performance is CPAM > NPAM > APAM. The ζ-potential of the MMT (001) surface increases under the action of three PAM, and the effect of CPAM is the most significant. The adsorption of PAM on the MMT (001) surface has the ability to neutralize the surface charge of MMT. The flocculation of MMT particles under PAM results in an increase of particle size and a decrease of specific surface area. Meanwhile, the pore volume of MMT decreases, and the average pore size increases. In addition, PAM mainly removes vicinal water on the MMT surface. The active sites of the MMT surface and PAM are calculated by DFT. The adsorption of three PAM structural units on the MMT Na-001 surface and non-001 surface is nonbonding interaction, and the adsorption energy of CPAM is the largest. And the left shift of ε_p of the O atom on the MMT surface is conducive to the stable adsorption of CPAM. The MD results show that the concentration of water molecules on the surface of MMT Na-001 decreases after PAM is adsorbed on the MMT Na-001 surface, indicating that PAM can keep water molecules away from the surface of MMT, which means that the hydrophobicity of the MMT surface is enhanced. This study has guiding significance for the selection of PAM and the development of new flocculants in the treatment of coal slime with a high content of MMT.

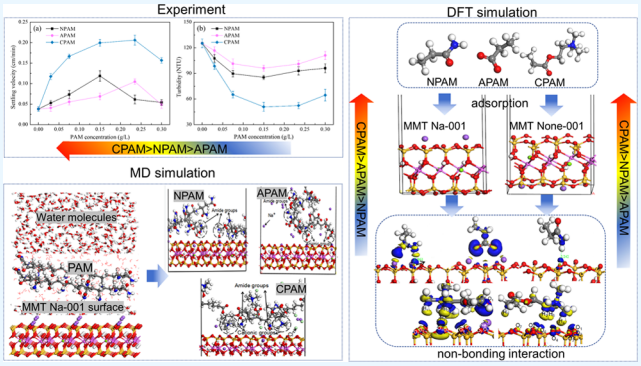

1. INTRODUCTION

With the deterioration of coal quality, the content of coal refuse in raw coal gradually increased, resulting in the production of a large number of clay minerals in the coal washing process.[1,2] Due to the high clay content and fine particle size, the filter cake has a high water content after coal mud press filtration, which cannot meet the requirements of subsequent coal mud use.[3,4] Therefore, reducing the water content of the filter cake is an urgent issue in most coal beneficiation plants. Common clay minerals found in coal slime water include quartz, kaolinite, montmorillonite (MMT), and illite. Compared to kaolinite and illite, MMT has a weaker interaction between the crystal layers and is more susceptible to water absorption, expansion, and sludge. In addition, due to lattice substitution, MMT has a large number of permanent negative charges, so clay minerals can adsorb a large number of ligand ions in water, forming a thick electric double layer, and the electrostatic repulsion between the double layers also occurs also due to the strong dispersion of MMT in water,[5] which leads to the difficulty of the coal slime settling and the high water of the filter cake in the pressure filtration.

Polyacrylamide (PAM) flocculants can accelerate the sedimentation of coal slime particles and improve the effect of pressure filtration. Therefore, it is widely used for coal slime water treatment.[6−8] PAM is a water-soluble organic polymer

Received: September 27, 2023
Revised: November 28, 2023
Accepted: December 6, 2023
Published: March 26, 2024

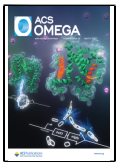

https://doi.org/10.1021/acsomega.3c07467
ACS Omega 2024, 9, 15818−15832

synthesized by copolymerization.[9] Based on their structures, PAM can be classified into nonionic polyacrylamides (NPAM), anionic polyacrylamides (APAM), and cationic polyacrylamides (CPAM), depending on the type of ion. The main reason that PAM can improve the sedimentation and pressure filtration of coal slime particles is that the flocculant stretches, bridges, and adsorbs fine particles, thereby forming flocs, so the gravitational force of the floc is greatly increased, accelerating its sedimentation rate.[3,10,11] At the same time, the effective particle size of the filter cake increases, which makes the permeability of the filter cake increase, so the pressure filtration rate is accelerated.[4] Adsorption of PAM structural elements onto hydrophilic clay particles is a premise for particle bridging. Therefore, it is of great importance to study the adsorption behavior of PAM structural elements on coal slime particles to explain the sedimentation and filtration mechanism.

In the study of the adsorption test of PAM on mineral surfaces, Fourier transform infrared spectroscopy, field-emission scanning electron microscopy, thermogravimetric analysis, quartz crystal microbalance with dissipation, X-ray diffraction, and ζ-potential are mainly used. A previous study by Wiśniewska et al.[12] measured the adsorption of APAM on the MMT surface using an ultraviolet visible spectrophotometer and found that APAM containing 5% −COOH group had greater adsorption capacity on MMT than APAM containing 30% −COOH group, which was thought to be due to electrostatic repulsion between the APAM and MMT surfaces. Mpofu et al.[13] studied an intermittent depletion method to measure the adsorption isotherm of APAM on kaolinite and deduced that the adsorption of APAM on kaolinite depends on hydrogen bonds. Macroscopically described effects of PAM on clay mainly include the following two aspects:[14−16] (1) PAM can be adsorbed on the clay surface through hydrogen bonding and electrostatic attraction and (2) PAM adsorbed on the clay surface can enhance the dehydration effect of clay.

The above research is very important for the efficient treatment of coal slime water. However, experimental studies are investigated at the nanoscale, and the explanation of the mechanism of interaction between agents and particles is mainly derived from macroscopic phenomena, so it is difficult to observe the process and the mechanism of a microscopic reaction between molecules. In order to avoid information loss due to insufficient resolution of experimental analytical instruments, density functional theory (DFT) methods have been widely used in recent years to study microscopic adsorption and the mechanism of organic matter and minerals.[17−19] The interaction of the MMT surface with small molecules has been extensively studied.[20−22] In addition, researchers have also studied the microscopic adsorption of polymer basic units to the surface of MMT.[23,24] However, the adsorption mechanism of PAM on MMT is not clear and needs further investigation.

In this study, first, the sedimentation tests of MMT and coal slime pressure filtration experiments were carried out, and ζ-potential, Brunauer−Emmett−Teller (BET) measurement, and low-field nuclear magnetic resonance detection were used to characterize the water content and form in the coal slime cake. Then, we analyzed the active sites of PAM structural units and the MMT (001) surface and analyzed the adsorption energy, charge differential density distribution, and charge transfer between them, which made it possible to understand the adsorption of PAM and MMT at the microscopic level. Lastly, the kinetic characteristics of the PAM polymer and water molecules on the surface of MMT Na-001 were calculated by molecular dynamics (MD), including the spatial distribution of water molecules and the self-diffusion coefficient of PAM. This work will be used to interpret macroscopic adsorption and flocculation experiments, contribute to a better understanding of the flocculation process, and provide useful information for molecular design and development of more effective flocculants.

2. SIMULATION CALCULATION METHODS

2.1. Samples and Reagents. Na-MMT was purchased from Shalin Shiyu Mineral Products Co., Ltd., Guzhang County, China. The particle size analysis results showed that the particle size was less than 200 mesh. The analysis result of the XRD spectrum is shown in Figure 1. The purity of MMT was 86%, containing a small amount of illite, quartz, feldspar, and other minerals.

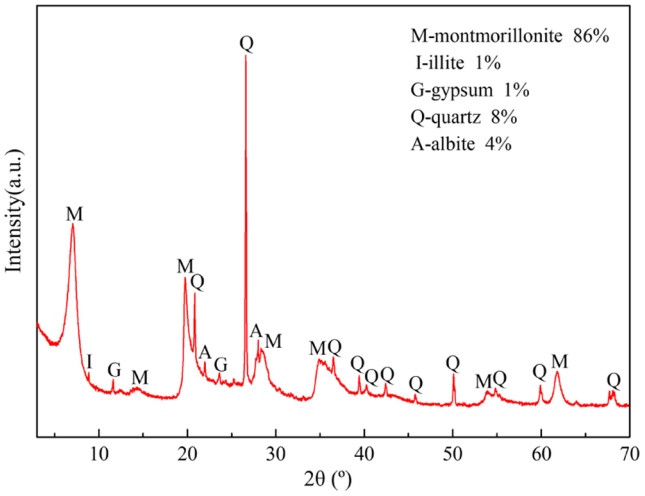

Figure 1. X-ray diffraction patterns of MMT.

The cleaned coal used in the test was heavy medium cleaned coal from a coal preparation plant in Ordos, China, which was bituminous coal. The bulk cleaned coal was subjected to floating−sinking tests, and samples with a density of less than 1.4 g/cm^3 were selected for grinding and grading to prepare cleaned coal samples with different particle sizes for later use. Table 1 shows the results of ash analysis of cleaned coal for each particle size. According to Table 1, the ash content of cleaned coal with different grain sizes was low, about 8%. The analysis of ash composition shows that it was mainly montmorillonite and a small amount of kaolinite.

Table 1. Ash Content of Cleaned Coal with Different Grain Sizes

particle size fraction (mm)	0.5−0.25	0.25−0.01	0.01−0.074	0.074−0.045
ash content (%)	7.89	7.55	8.31	8.63

Nonionic polyacrylamide (NPAM) (12 million), anionic polyacrylamide (APAM) (12 million), and cationic polyacrylamide (CPAM) (12 million) were used as flocculating filter aids with a configured concentration of 1.5 g/L.

https://doi.org/10.1021/acsomega.3c07467
ACS Omega 2024, 9, 15818−15832

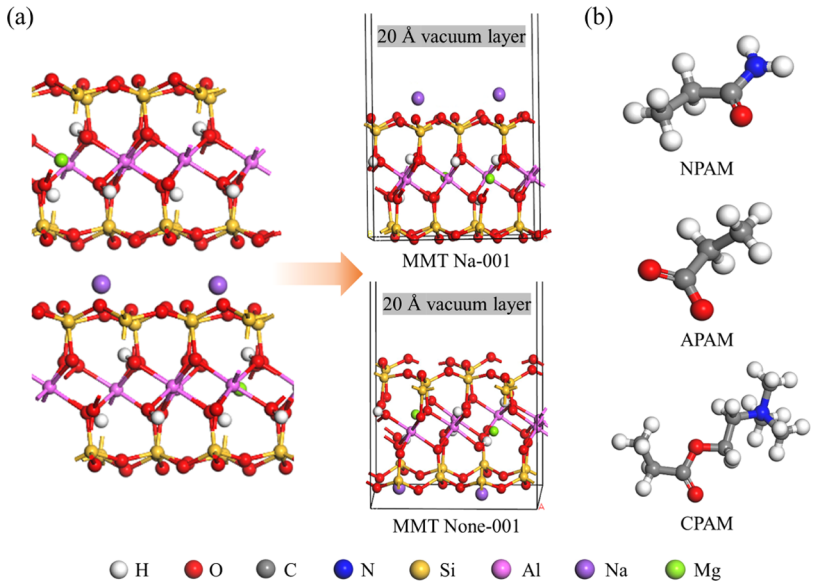

Figure 2. (a) Surface models of MMT cell, Na-001, and None-001 of MMT and (b) structural units of three PAM.

2.2. Sedimentation Experiments. *2.2.1. Settlement Experimental Method.* First, a graduated paper was affixed vertically to the outside wall of a 100 mL cylinder, and then the MMT suspension (concentration of 10 g/L) was poured into the measuring cylinder (15 mmol/L $CaCl_2$ was added to simulate real aqueous solution), and a certain amount of PAM was added. Lastly, the cylinder was turned over vertically in both directions five times to fully mix PAM with MMT suspension. At this time, the water−solid interface was taken as the target position, and the time was recorded every 4 cm to calculate the sedimentation velocity according to the stage of a rapid drop of solid particles. After settling test, 30 mL of the upper supernatant 5 cm below the liquid surface was with a pipet, and the turbidity was measured by a turbidity meter.

2.3. Vacuum Filtration Experiments. *2.3.1. Vacuum Filtration Test.* Cleaned coal with a particle size of less than 0.074 mm and MMT were mixed at a mass ratio of 9:1 as coal slime, and then coal slime with a mass concentration of 100 g/L was prepared. It was soaked for 10 h before PAM was added. Filtration was ensured through a vacuum filter plate of diameter 13 cm with filter paper (30−50 μm). After repeated experiments, the weight of the filter cake was recorded when the weight of the filter cake changed little, and the water content of the filter cake was calculated as shown in eq 1

$$P = M/(M + s) \quad (1)$$

where P is the water content of the filter cake, M is the water content of the coal slime filter cake, and s is the mass of the dried coal slime.

2.4. ζ-Potential Measurements. ζ-potential of coal slime water after adsorption of different kinds of PAM was measured using a Zeta phoremeter. After PAM was added, the coal slime water suspension was left for 10 min, and the supernatant containing colloidal particles was injected into an electrophoresis tank by using a syringe. The movement trajectories of about 100 particles were tracked by laser illumination and a CCD imaging system. At the same time, the instrument system software converted the electrophoretic mobility value into the ζ-potential value based on the Smoluchowski equation, so as to obtain the ζ-potential distribution of these particles. Each sample was averaged after three measurements.

2.5. BET Measurements. The specific surface area and pore characteristics of dry montmorillonite samples before and after PAM adsorption were analyzed by automatic specific surface area and pore analysis (Micromeritics ASAP 2460). The pretreatment conditions were 70 °C and 8 h. The specific surface area and total pore volume of montmorillonite samples before and after PAM were measured by the Brunauer−Emmett−Teller technique. The aperture distribution was determined by using the Barrett−Joyner−Halenda method.

2.6. Low-Field Nuclear Magnetic Resonance (LF-NMR) Measurements. A high-precision magnetic resonance SOIL analyzer (SoIL-2260) was used to detect the water form of the filter cake. The measured parameters were as follows: CPMG detection pulse, G302201 detection probe, and sample height of 10 mm. Based on the calibration of the standard sample (original sample), the water content and spatial characteristics of the filter cake obtained under different experimental conditions were determined and the sample relaxation attenuation curve was obtained. Then, the T2 distribution was obtained according to the band-residual difference (BRD) inversion algorithm. The effect of inversion was judged by the forward processing of the signal, the forward data was compared with the inverted data, and the fitting degree was less than 99.9% for retest.

2.7. DFT Calculations. DFT calculation was performed by using the DMol[3][25] module and CASTEP[26,27] module of Materials Studio 2017 software (Accelrys, San Diego, USA). MMT crystal cell parameters were a = 5.29 Å, b = 9.01 Å, c = 9.5 Å, α = 91.02°, β = 101.79°, and γ = 89.84°. Every eight Al in the model was replaced by one Mg, and the cation Na was added between the layers. The original unit cells were expanded (2 × 1 × 1) and then cut along the surface of (001) to form (001) surfaces with and without Na (Na-001 surface and None-001 surface). A vacuum layer (20 Å) was added to the MMT surface to avoid interaction between the surface and the bottom layer.[28] MMT and its (001) surface-optimized model are shown in Figure 2a. The three PAM structure units are based on the refs 29−31 (Figure 2b). In this

https://doi.org/10.1021/acsomega.3c07467
ACS Omega 2024, 9, 15818−15832

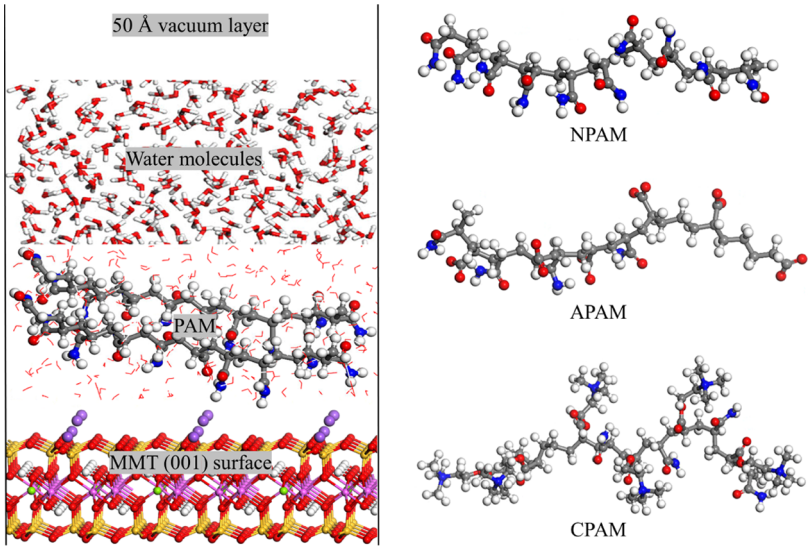

Figure 3. Initial adsorption model of PAM on the MMT Na-001 surface in aqueous solution.

paper, the structural units of three kinds of polyacrylamide were expressed in the same way as the long chain of polyacrylamide, namely, NPAM, APAM, and CPAM.

The energy band structure and density of states of the MMT (001) surface were calculated by the CASTEP module. The GGA-PBE[32] exchange correlation function was used to accurately describe hydrogen bonds,[33,34] and TS dispersion correction was added, the plane wave truncation energy was 410 eV, and the *k*-point sampling grid was 2 × 2 × 1.[35] The lattice parameters of the optimized MMT were a = 10.45 Å and b = 9.07 Å, which are close to the experimental values of a = 10.32 Å and b = 8.96 Å,[36] which proves the reliability of the optimized parameters.

The frontier molecular orbitals of three PAM were calculated by the DMol^3 module.[37]

PAM was placed on different sites on the surface of MMT (001) for optimization, and the stability of the adsorption system was analyzed after calculating the adsorption energy. The strength of the interaction between the adsorbent and adsorbate can be judged by the adsorption energy.[38] The adsorption energy was defined as the difference between the total energy after and before adsorption of PAM and the MMT (001) surface.

The adsorption energy of PAM on the surface of MMT (001) was calculated as follows eq 2

$$E_{ads} = E_{system1} - E_{system2} \quad (2)$$

where E_{ads} is the adsorption energy and $E_{system1}$ is the total energy of the system when PAM is adsorbed on the surface of MMT (001). $E_{system2}$ is the total energy of the system when PAM is away from the surface of MMT (001), and the PAM of this system does not adsorb with the surface of MMT (001).

The p-band center (ϵ_p) of O has been proved to have a large effect on the adsorption energy of the reactive intermediates.[39] In this report, the concept of the upper p-band edge, ε_p, is defined as the highest peak position of the Hilbert transform of the projected density of states (PDOS) onto p-orbitals eq 3

$$\varepsilon_p = \frac{\int_{-\infty}^{\infty} n_d(\varepsilon)\mathrm{d}\varepsilon}{\int_{-\infty}^{\infty} n_d(\varepsilon)\mathrm{d}\varepsilon} \quad (3)$$

where ε is the energy level and $n_p(\varepsilon)$ is the density of states.

2.8. MD Calculations. The MMT single-crystal cell was expanded into the MMT supercrystal cell (2 × 3 × 1), and the MMT Na-001 surface was obtained by sectioning along the (001) surface. 1000 water molecules (50 Å, ρ = 0.98 g/cm^3) and two PAM molecules were added to the system; then, a 50 Å vacuum layer was set on top of the water molecule layer to prevent the interference phenomenon of the periodic mirror layer on the interface adsorption. The PAM studied in this work includes NPAM, APAM, and CPAM, in which NPAM consists of ten acrylamide groups, APAM is the acrylamide after partial carboxylic acid group substitution, and CPAM is the acrylamide after quaternary ammonium group substitution.[40] The substitution rate of ionic groups for both APAM and CPAM was 60%, and then, PAM was geometrically optimized in the CASTEP module. The initial adsorption model of PAM at the solid−liquid interface of MMT in aqueous solution environment is shown in Figure 3.

Molecular dynamics (MD) simulation calculations of PAM adsorption on the MMT Na-001 surface were investigated using the Forcite module of Materials Studio 2017 software. The conjugate gradient method was used to optimize the geometry of the system. The Berendsen function was used for pressure control, and the Nosé function was used for temperature control. Long-range electrostatic and van der Waals interactions were calculated using the Ewald method and Atom-based methods, respectively, and the cutoff distance was 10 Å. After assigning the PCFF-INTERFACE force field to each atom, the calculation was first performed under the NPT ensemble for 100 ps with a step of 0.2 fs, and then the last frame of the system was selected for the 1 ns equilibrium calculation under the NPT ensemble with a step of 1 fs. The convergence curves of the energy and temperature over time were monitored to ensure equilibrium. Data were collected every 100 ps, and the calculated results of the last 500 ps were selected for molecular dynamics analysis.

The interaction energy between PAM and the MMT Na-001 surface was calculated according to the simulation results, as shown in eq 4

https://doi.org/10.1021/acsomega.3c07467
ACS Omega 2024, 9, 15818−15832

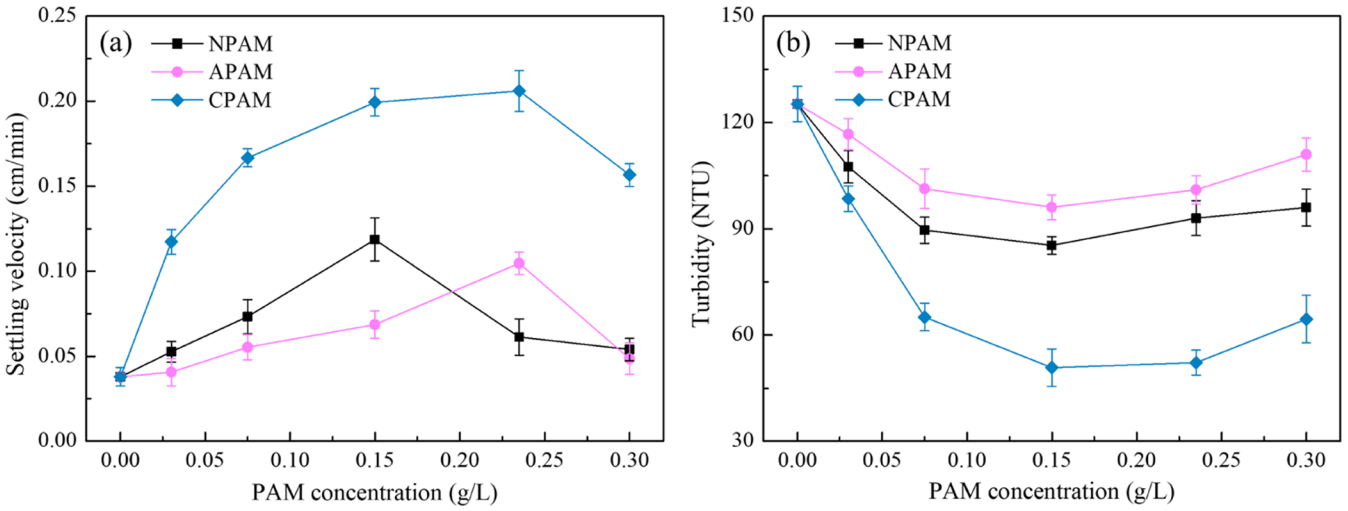

Figure 4. Settlement effect of MMT suspension under three PAM: (a) Settlement velocity and (b) turbidity.

$$E_{ads} = (E_{system} - E_{PAM} - E_{surface} - E_{p+W} - E_{s+W} + E_{water} + E_{p+s})/2 \quad (4)$$

where E_{system} is the energy of the whole system, E_{PAM}, $E_{surface}$, and E_{water} are the energies of PAM, the MMT Na-001 surface, and water molecules respectively, E_{p+W} is the interaction energy between PAM and water molecules. E_{s+W} is the interaction energy between water molecules and the MMT Na-001 surface, and E_{p+s} is the interaction energy between PAM and the MMT Na-001 surface.

Mean square displacement (MSD)[41] was used to describe the deviation of the spatial position of the target particle from the initial position with the change of time. The calculation method was as follows eq 5

$$MSD = \langle |r(t) - r(0)|^2 \rangle \quad (5)$$

where r(t) is the particle position at time t and $r(0)$ is the particle position at initial time.

Diffusion coefficient (D) is a physical parameter characterizing the diffusion degree of the target ion, which can be obtained by the Einstein relation,[42] as shown in eq 6

$$D = \frac{1}{6N} \lim_{t\to\infty} \frac{d}{dt} \sum_{I=1}^{N} \langle [|r_i(t)| - |r_i(0)|]^2 \rangle \quad (6)$$

where $r_i(0)$ and $r_i(t)$ are the position vectors of PAM at time t = 0 and time t, respectively, and N is the number of PAM.

3. RESULTS AND DISCUSSION

3.1. Settlement Results. The settlement test results of the MMT suspension at three different amounts of PAM are shown in Figure 4. Figure 4a shows that all PAM can effectively improve the settling velocity of solid particles in the MMT suspension. The sedimentation velocity increased first and then decreased with the increase of PAM concentration. The greater the concentration of PAM is not the better, that is, there is a reasonable range. The possible reason is that when the amount of PAM is too much, the PAM molecular chains will wrap around each other, reducing the hydrophobicity of the mineral surface.[43,44] The maximum sedimentation velocities under the three PAM were 0.119 cm·min^{-1} (NPAM), 0.105 cm·min^{-1} (APAM), and 0.206 cm·min^{-1} (CPAM), respectively. From the measurement results of the turbidity of the supernatant (Figure 4b), it can be seen that the turbidity of the supernatant decreases after the addition of PAM. Among them, CPAM has the most obvious effect, and the turbidity can be greatly reduced to 50.8 NTU by adding 0.15 g/L CPAM. In summary, the ability of the three PAM to improve the settlement effect of the MMT suspension is CPAM > NPAM > APAM.

3.2. Vacuum Filtration Results. The experimental results of vacuum pressure filtration of artificially mixed coal slime water at three different amounts of PAM are shown in Figure 5. It showed that for the three PAM, the water content of the coal slime after filtration first decreases and then increases with the increase of the concentration. When the concentration of NPAM was 0.15 g/L, the minimum water content of coal slime was 44.15%, and when the concentration was increased to 0.235 g/L, the water content was increased to 47.45%. The effect of APAM concentration on coal slime pressure filtration was basically the same as that of NPAM. The effect of CPAM was significantly better than that of NPAM and APAM. When the concentration of CPAM was 0.03 g/L, the water content of

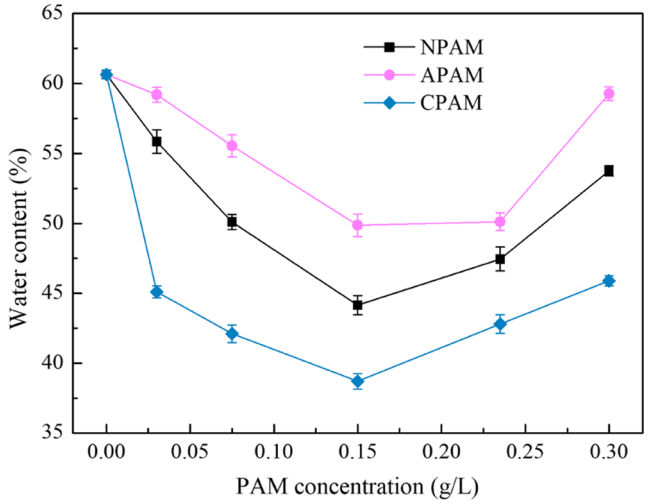

Figure 5. Vacuum filtration test results of coal slime water under three PAM.

https://doi.org/10.1021/acsomega.3c07467
ACS Omega 2024, 9, 15818−15832

the coal slime was 45.10%. The water content of coal slime was further reduced by increasing the PAM concentration. The optimum concentration of CPAM was 0.15 g/L, and the coal slime water content was reduced to 38.70%. In addition, it was observed in the experimental process that the filtration time of coal slime after adding CPAM was significantly shorter than that of NPAM and APAM, which indicates that CPAM can improve the filtration efficiency of coal slime water, which is very favorable for actual coal production.

In conclusion, the improvement effect of three PAM on coal slime water pressure filtration was in the order CPAM > NPAM > APAM. The results of the sedimentation test and vacuum pressure filtration test showed that CPAM has the best effect.

3.3. ζ-Potential Analysis. Charge transfer occurs when PAM is adsorbed on the MMT surface; that is, PAM can improve the treatment effect of coal slime water by changing the charging situation on the MMT surface. The adsorption effect of PAM on the MMT (001) surface was analyzed from a macroscopic point of view by measuring ζ-potential, and the results are shown in Figure 6.

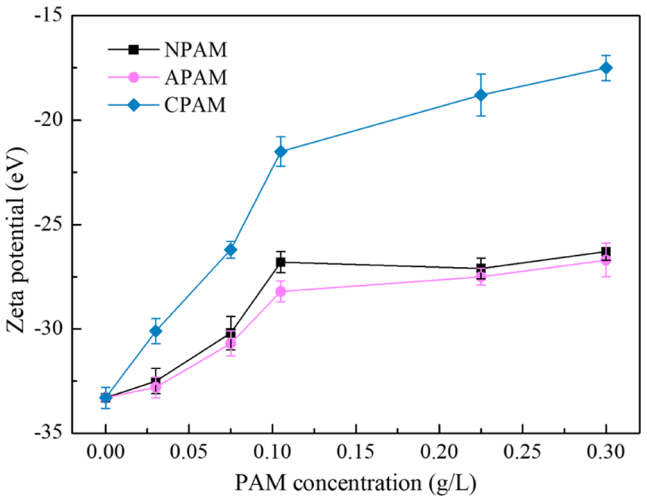

Figure 6. Effect of three PAM on the ζ-potential of coal slime particles.

Figure 6 shows that the Zeta value of the coal slime particle is −33.3 eV when PAM is not added. The reason for the higher electronegative surface of slime particles is that the surface of coal has electronegative hydroxyl and carboxyl functional groups, and MMT has a large number of negative charges between layers due to the isomorphic substitution.[45] The ζ-potential increased slightly with the increase in the concentration of NPAM and APAM, indicating that the adsorption of NPAM and APAM by MMT increased. NPAM and APAM mainly flocculate in the sedimentation and filtration process of coal slime water; at the same time, the adsorption of NPAM and APAM on the MMT surface can compress the double layer effectively to a certain extent.[46,47] When the concentration of CPAM increased, the ζ-potential increased significantly, indicating that the negativity on the surface of the coal slime particles was weakened. When the concentration of CPAM increased to 0.3 g/L, the ζ-potential was −17.5 eV. Compared with NPAM and APAM, CPAM plays a flocculating role in the adsorption of the MMT surface and also has the effect of neutralizing its surface charges. Shaikh et al.[48] measured the ζ-potential of bentonite with CPAM, and Nasser et al.[49] measured the ζ-potential of kaolinite with CPAM. Both showed that ζ-potential increased with the increase of PAM concentration, which was consistent with the measured results of this experiment.

3.4. BET Analysis. The specific surface area and pore characteristics of MMT before and after adsorption of three different kinds of PAM are shown in Table 2. The specific surface area of MMT without PAM adsorption was 17.6125 m^2/g. In contrast, the specific surface area of MMT adsorbed after three PAM decreased significantly, and the decrease was the most significant after adsorption of CPAM, which was 7.7933 m^2/g. The flocculation of MMT particles under the action of PAM results in the increase of particle size and the decrease of specific surface area of the particles. The variation of specific surface area of MMT by PAM species is consistent with the results of sedimentation and filtration tests. The change of specific surface area of MMT is directly related to the change of pore characteristics. The total pore volume of MMT decreases and the average pore size increases after PAM adsorption. The possible reason is that under the action of PAM, the fine particles will enter the pores between the coarse particles for different degrees of filling, resulting in an increase in the pore size and a corresponding decrease in the pore volume. The average pore size of MMT after PAM adsorption was CPAM (130.051 Å) > NPAM (125.377 Å) > APAM (123.819 Å). The degree of influence of PAM on the pore characteristics of MMT is consistent with the variation of specific surface area.

Table 2. BET Specific Surface Area and Pore Parameters before and after PAM Adsorption by MMT

flocculant	BET specific surface area (m^2/g)	total pore volume (cm^3/g)	average pore diameter (Å)
none	17.6125	0.041770	94.864
NPAM	8.4982	0.026551	125.377
APAM	8.7143	0.026975	123.819
CPAM	7.7933	0.025338	130.051

3.5. LF-NMR Analysis. Water in the filter cake includes the water of hydration, vicinal water, and interstitial water.[50] In order to study the influence of PAM on the water occurrence state on the surface of the filter cake, the T2 relaxation distribution spectrum of the filter cake under the optimal concentration of three PAM was analyzed, respectively, and the results are shown in Figure 7.

Three types of water in the T2 relaxation time of feature maps the range of T2 correspond to 0.01−0.45, 0.45−100, and >100 ms. Figure 7 shows that for 0.01−0.45 ms, the T2 signal detected showed that adding PAM on the coal slime cake did not affect the form and content of the water of hydration. When PAM was not added, T2 had almost no signal detected in the region greater than 100 ms, indicating that there was almost no interstitial water in the filter cake, that is, this result indicated that the interstitial water can be basically removed by only mechanical filtration. The T2 signal detected within 0.45−100 ms represents vicinal water in the coal slime cake. After adding PAM, T2 within 0.45−100 ms had a great change of vicinal water, indicating that PAM in MMT surface adsorption is mainly vicinal water away from the surface of the water molecules. The size of T2 can reflect the degree of freedom of water molecules in the filter cake. The larger T2

https://doi.org/10.1021/acsomega.3c07467
ACS Omega 2024, 9, 15818−15832

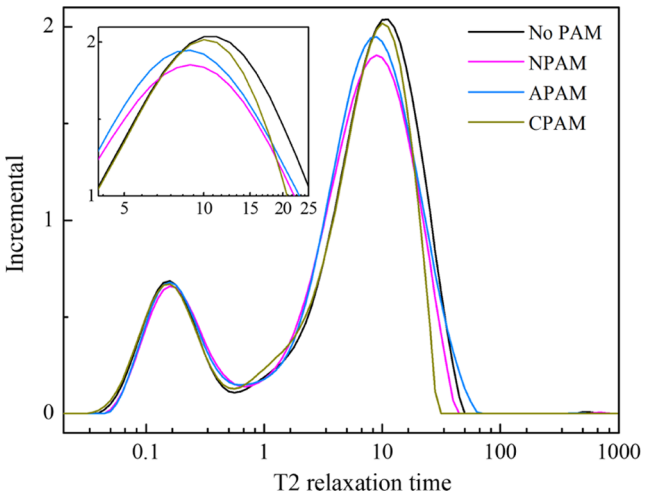

Figure 7. T2 relaxation distribution spectrum of the filter cake after PAM.

was, the greater the degree of freedom of water molecules and the weaker the binding effect of water molecules.

The vertex position of the peak and the area of the peak were calculated for the T2 curve in Figure 7, and the proportion of vicinal water and water of hydration on the MMT surface under the effect of PAM was further quantified and analyzed. The results are shown in Table 3, and the peak

Table 3. T2 Spectral Information on Water Content of the Filter Cake

flocculant	location of the top of the T2 peak in vicinal water (ms)	T2 peak area of the water of hydration	T2 peak area of vicinal water	proportion of T2 peak area in vicinal water (%)
none	10.00	8.14	36.20	81.64
NPAM	7.94	8.13	33.90	80.66
APAM	7.94	8.14	36.00	81.56
CPAM	8.91	8.17	32.11	79.72

areas of the water of hydration in MMT without PAM and after the addition of the three PAM were almost the same. Without PAM, the proportion of vicinal water was 81.64%. The proportion of vicinal water decreased after PAM addition, and the proportion of vicinal water after three kinds of PAM was 80.66% (NPAM), 81.56% (APAM), and 79.72% (CPAM), respectively. In addition, it can be seen from the position of the peak point that the position of the peak point was 10 ms when PAM was not added. After PAM was added, the position of the peak point moved to the left, indicating that the degree of freedom of water molecules adsorbed by MMT was reduced under the action of PAM.

Based on the above results, PAM can remove the vicinal water on the MMT surface by flocculation, and its removal ability was in the order CPAM > NPAM > APAM. When PAM was adsorbed on the MMT surface, the floc formed by PAM molecules will enclose a certain amount of water molecules, which were difficult to discharge. At the same time, the PAM molecules on the surface of MMT can form a dense adsorption layer on its surface and cannot enter between the MMT layers, so the vicinal water between the MMT layers cannot be effectively removed.[51,52]

3.6. DFT Calculation Results. *3.6.1. Active Sites and Reactivity.* The band structure and density of states of MMT are shown in Figure 8. According to Figure 8a, the energy band of the MMT crystal was composed of five parts. The Fermi level is set at 0 eV, the energy band below the Fermi level is the valence band, the energy above the Fermi level is the conduction band, the energy at the top of the valence band is 0 eV, and the energy at the bottom of the conduction band is 5 eV. To understand the atomic occupancy at the top and bottom of the valence band, the total density of states (TDOS) of the MMT surface and the partial wave density of states (PDOS) of each atom were calculated, and the results are shown in Figure 8b−h. It was known that the top position of the valence band was mainly contributed by the 2p orbital of the O atom, and the bottom position of the conduction band was mainly contributed by the 2s orbital of the Na atom. The top of the valence band and the bottom of the conduction band correspond to the highest occupied crystal orbital (HOCO) and the lowest unoccupied crystal orbital (LUCO) of the crystal, respectively.[53] Therefore, the O atom and Na atom are active sites. This result is identical to the simulation result obtained by Peng.[35] There is no Na atom on the surface of MMT None-001, so its active site is the O atom.

The properties of a molecule are mainly determined by the front molecular orbitals, namely, the highest occupied orbital (HOMO) and the lowest unoccupied orbital (LUMO). The results of the front track analysis of the three PAM are shown in Figure 8i. It can be seen from Figure 8i that most of the front orbits of NPAM, APAM, and CPAM groups were distributed on the O atoms. Meanwhile, according to the specific data of Fukui functions of the three PAM in Appendix (Table S1), it can be seen that the largest Fukui (+) and Fukui (−) values of the three PAM were all O atoms, so the active sites of the three PAM are all O atoms. The results are consistent with those reported in related study.[54]

The ease of interaction between minerals and agents can be measured in terms of the energy difference between the highest occupied orbital HOMO/HOCO of the electron donor and the LUMO/LUCO of the electron acceptor. The smaller the absolute value of the energy difference ($|\Delta E|$), the stronger the interaction between the mineral and agent. The results of the energy difference of the frontier orbitals between PAM and MMT are shown in Table 4, where $|\Delta E_1|$ is the absolute value of the difference between the HOMO of PAM and the LUCO of the MMT Na-001 surface, $|\Delta E_2|$ is the absolute value of the difference between the LUMO of PAM and the HOCO of the Na-001 surface, $|\Delta E'_1|$ is the absolute value of the difference between the HOMO of PAM and the LUCO of the MMT None-001 surface, and $|\Delta E'_2|$ is the absolute value of the difference between the HOCO of the None-001 surface and the LUMO of PAM. When the energy level difference between the HOMO/HOCO and LUMO/LUCO of the two substances is less than 6 eV, the electron transition occurs between the two orbitals.[55,56] Table 4 shows that the electrons of NPAM and APAM easily transition to the MMT (001) surface. However, the electrons on the MMT (001) surface were easy to transition to CPAM. The reaction activity of PAM with the Na-001 surface and None-001 surface of MMT was CPAM > APAM > NPAM and CPAM > NPAM > APAM.

3.6.2. Adsorption Configuration and Energy. The optimal adsorption configurations of NPAM, APAM, and CPAM on the MMT Na-001 surface and None-001 surface are shown in Figure 9. NPAM tends to adsorb on the MMT Na-001 surface, mainly because the O atom of NPAM attracts the Na atom on the MMT Na-001 surface, and the O atom of NPAM is

https://doi.org/10.1021/acsomega.3c07467
ACS Omega 2024, 9, 15818−15832

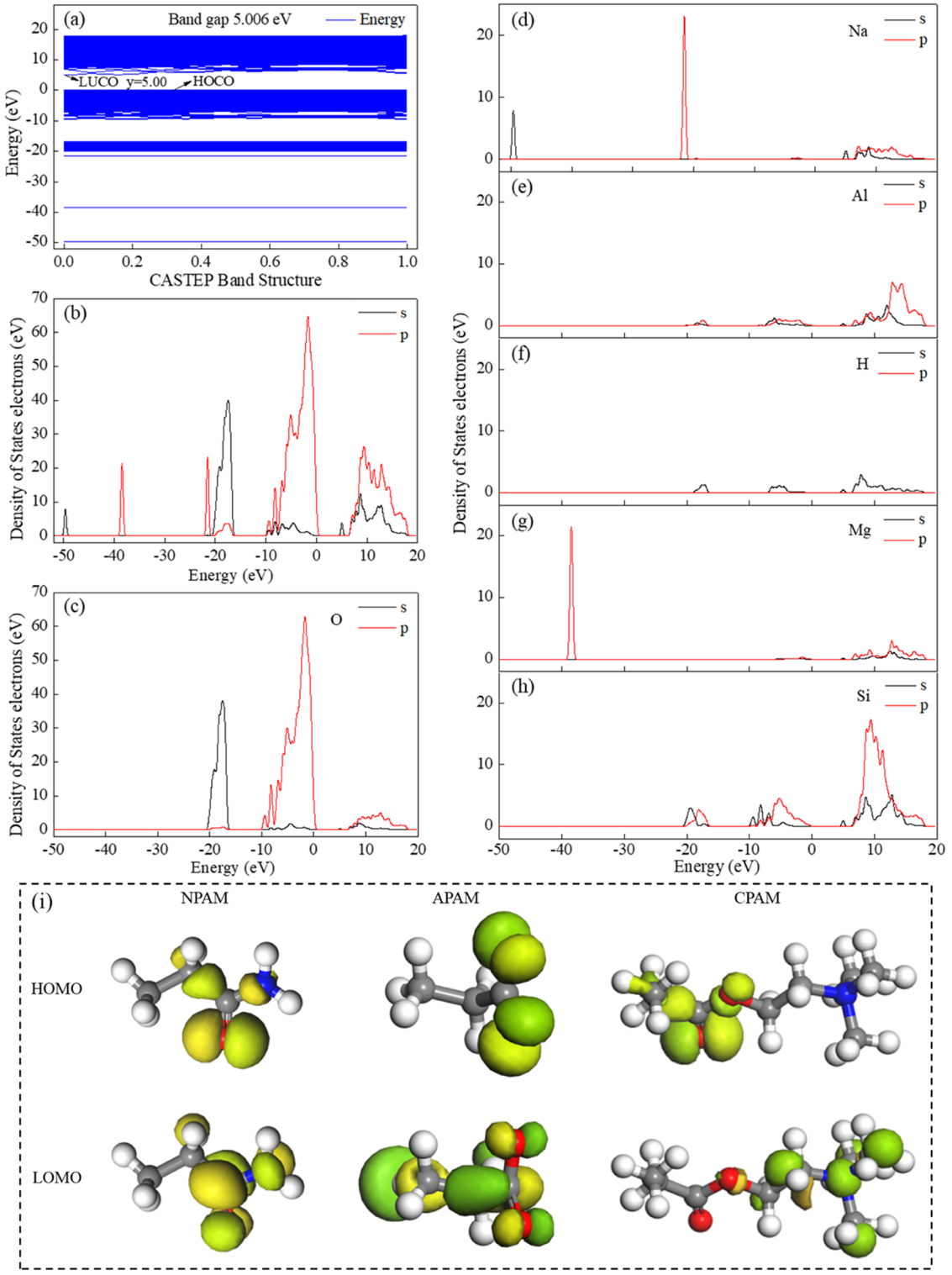

Figure 8. (a) Energy band of MMT; (b) TDOS of MMT; (c–h) PDOS of each atom; and (i) frontier molecular orbitals of the three types of PAM.

relatively far from the MMT None-001 surface due to the large local negative charges on the surface. For APAM, the optimal adsorption configuration exists only on the Na-001 surface.

The reason why APAM did not have a stable adsorption configuration on the None-001 surface may be that the local negative charges on its surface generate electrostatic repulsion on APAM, which causes APAM to move away from the MMT (001) surface. The O atoms tend to be adsorbed on the MMT Na-001 surface, and the two O atoms were symmetrically adsorbed on the two Na atoms on the surface. When CPAM was adsorbed on the surface of MMT, the interaction between them was strong due to the opposite charges. In addition, according to the space distance of PAM adsorption on the MMT (001) surface, it can also be intuitively seen that the space distance of CPAM was significantly reduced compared to

https://doi.org/10.1021/acsomega.3c07467
ACS Omega 2024, 9, 15818−15832

Table 4. Frontier Orbital Energies and the HOMO/LUMO Gaps of PAM and MMT Na-001 Surface and None-001 Surface

compute object	HOMO (eV) HOCO (eV)	LOMO (eV) LOCO (eV)	$\|\Delta E_1\|$ (eV)	$\|\Delta E_2\|$ (eV)	$\|\Delta E_1'\|$ (eV)	$\|\Delta E_2'\|$ (eV)
NPAM	−5.90	−0.12	3.47	6.92	3.41	7.26
APAM	1.00	5.55	3.43	12.59	3.49	12.93
CPAM	−9.21	−3.99	6.78	3.05	6.72	3.39
Na-001	−7.04	−2.43	-	-	-	-
none-001	−7.38	−2.49	-	-	-	-

those of NPAM and APAM, indicating that CPAM has the most significant adsorption effect on the MMT (001) surface.

In order to have a more specific understanding of the adsorption strength of different PAM on the MMT surface, a quantitative analysis was carried out by calculating the adsorption energy of both, and the results are shown in Table 5. According to Table 5, the adsorption energy of NPAM and APAM on the MMT surface was less than −1.0 eV, while the adsorption energy of CPAM was higher and the highest was −3.94 eV. The results of adsorption energy calculation were consistent with the rule of optimal adsorption configuration analysis. At the same time, the adsorption energy of NPAM and CPAM on the None-001 surface was greater than that on the Na-001 surface, while APAM could not be adsorbed on the None-001 surface.

3.6.3. Differential Charge Density. The electron transfer during PAM adsorption on the MMT surface was explored, and the differential charge densities of the optimal adsorption configuration (Figure 10) and the Hirshfeld charge before and after adsorption (Table S2) were calculated. Figure 10 shows that there was an obvious electron transfer during the adsorption of the three PAM with the MMT (001) surface. The least charge transfer occurs when NPAM was adsorbed on the MMT (001) surface. NPAM transferred 0.06 electrons to the Na-001 surface, None-001 surface transferred 0.08 electrons to NPAM, and APAM transferred 0.42 electrons to the Na-001 surface. When CPAM was adsorbed on the MMT Na-001 surface and None-001 surface, there was a large amount of electron transfer, and 0.36 electrons and 0.10 electrons were obtained from the MMT (001) surface, respectively.

Table 5. Adsorption Energy of PAM Structural Units on the MMT Surface

PAM type	NPAM		APAM	CPAM	
MMT surface	Na-001	none-001	Na-001	Na-001	none-001
adsorption energy/eV	−0.63	−0.22	−0.85	−2.55	−3.94

Table S2 details the Hirshfeld charge transfer before and after the adsorption of PAM on the MMT surface. For NPAM and the MMT Na-001 surface, the electron cloud accumulated near the O_2 ion of MMT (001) was shifted to NPAM, the positive charges of H_1 decreased, and the negative charges of O_2 decreased. The length of the H_1-O_2 bond was 1.861 Å, which was less than the sum of the radius of H and O atoms (2.65 Å). So, a N−H···O hydrogen bond was formed. At the same time, the electron cloud accumulated around the O_1 ion of NPAM was shifted to the Na-001 surface, the negative charges of the O_1 decreased, the positive charges of the Na_1 decreased, and the solitary pair electrons on the O_1 ion migrated to the empty orbital of the Na_1 ion, so there was a coordination interaction between O_1 and Na_1. For NPAM and MMT None-001 surface, the electron cloud accumulated that the O_1 ion on the None-001 surface shifted to NPAM, the positive charges of H_1 decreased, the negative charges of O_1 decreased, and the bond length of H_1-O_1 was 2.242 Å. Therefore, NPAM also formed N−H···O hydrogen bond when it adsorbed on the None-001 surface. For the surface of APAM and MMT Na-001 surface, the electron cloud accumulated around the O ion of APAM simultaneously shifted to the Na-001 surface, which was due to the existence of solitary pairs of electrons on the O ion of APAM, which migrated to the empty orbital of Na ion, so there was a coordination interaction between O_1 and Na_1 and O_2 and Na_2. The negative charges of O_1 and O_2 were reduced by 0.14e and 0.12e, respectively, and the positive charges of Na_1 and Na_2 were reduced by 0.06e and 0.08e, respectively. Besides the electrostatic interaction between H and O, there was also the coordination interaction between the lone pair electron of the O_1 ion and the empty orbital of the Na_1 ion between CPAM and the Na-001 surface. Electrostatic interaction was the main form of adsorption between CPAM and the None-001 surface. The above simulation results can well explain the differences of the three PAM adsorption on the MMT (001) surface from the perspective of electron transfer during adsorption.

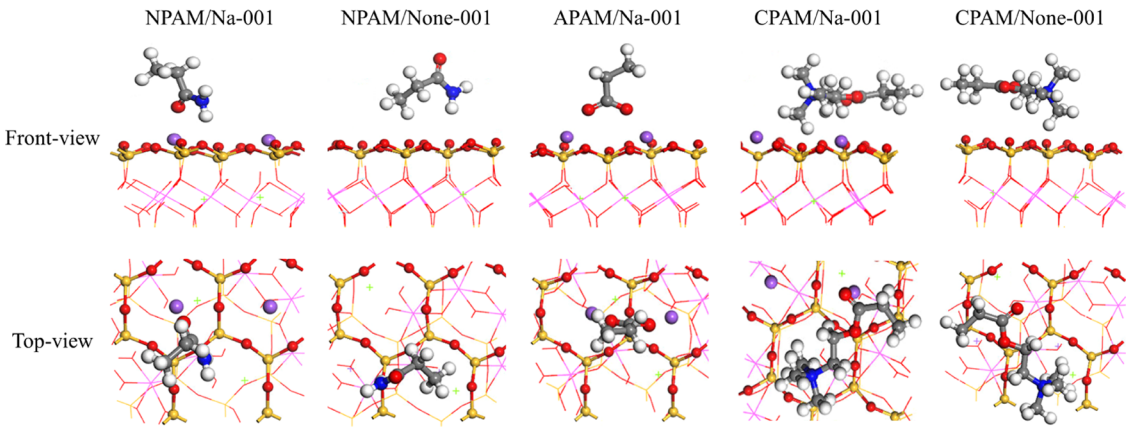

Figure 9. Optimal adsorption configurations of three PAM structures on the surfaces of MMT Na-001 and None-001.

https://doi.org/10.1021/acsomega.3c07467
ACS Omega 2024, 9, 15818−15832

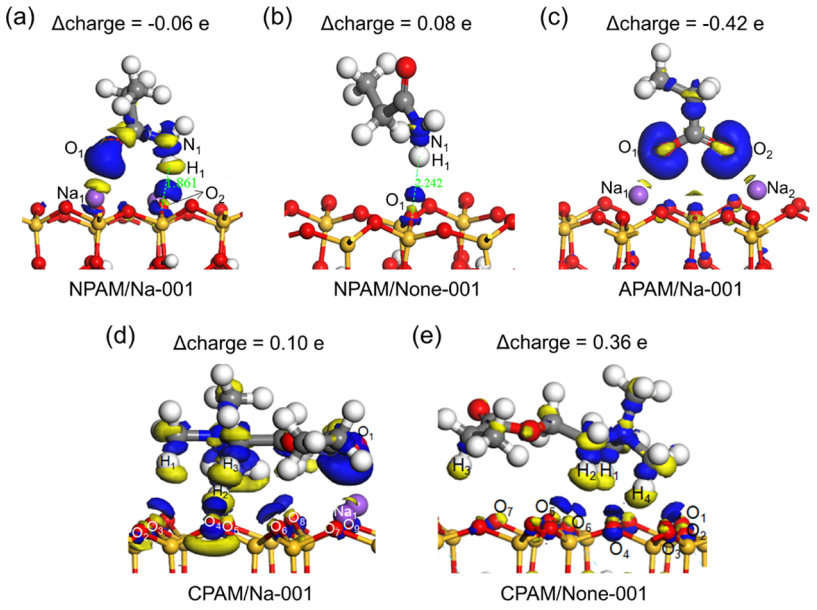

Figure 10. Differential charge density of NPAM on MMT: (a) Na-001 surface and (b) None-001 surface. Differential charge density of APAM on MMT: (c) Na-001 surface. Differential charge density of CPAM on MMT: (d) Na-001 surface and (e) None-001 surface. ΔCharge is the total charge change of PAM before and after adsorption on the MMT surface. Yellow is electron density dissipation. Blue is electron density accumulation.

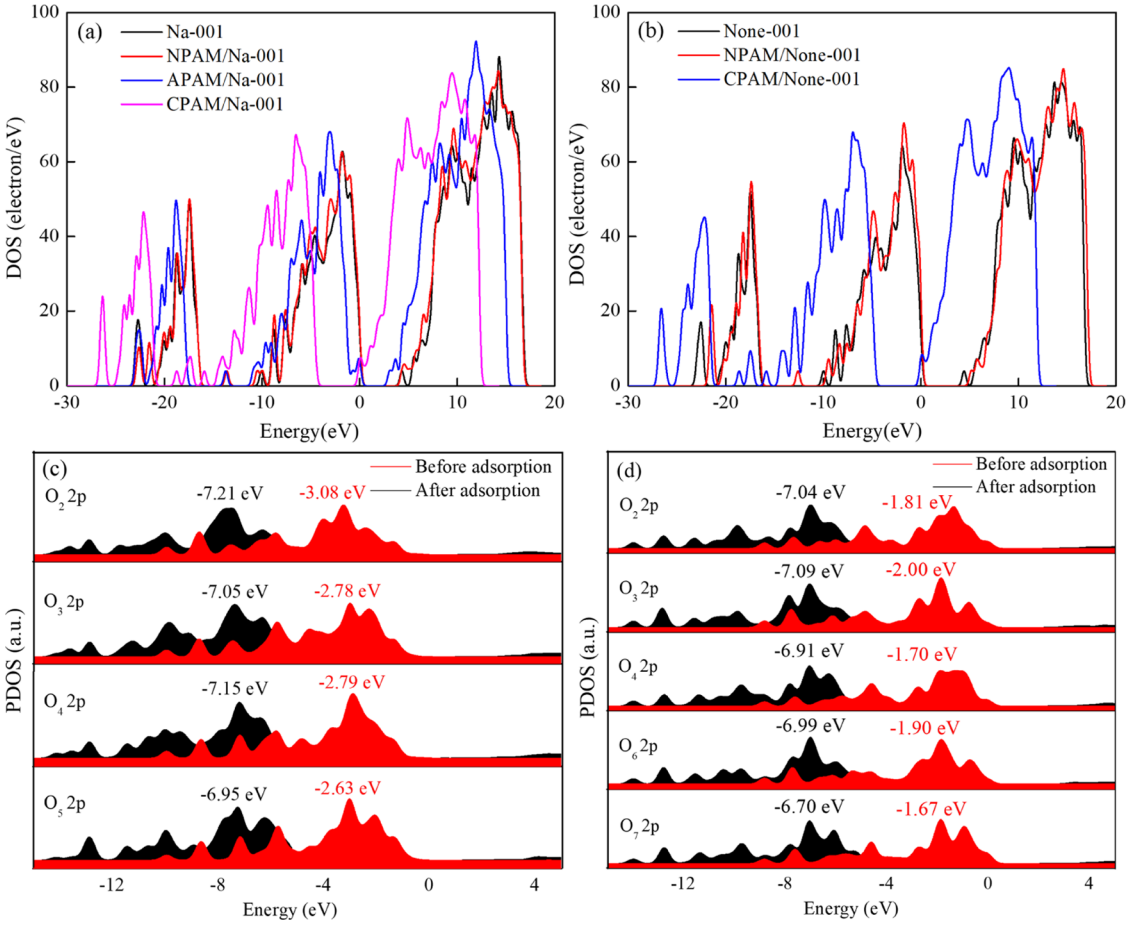

Figure 11. DOS of three PAM structural units adsorbed on MMT: (a) Na-001 and (b) None-001 surface in the optimum adsorption system. PDOS of O atoms on MMT (c) Na-001 and (d) None-001 surface, ϵ_p showed on the peak.

3.6.4. Density of States Analysis. Figure 11a,b shows the DOS after adsorption of three PAM on the surface of MMT Na-001 and None-001, respectively. It can be seen that the DOS distribution range of MMT Na-001 before PAM

https://doi.org/10.1021/acsomega.3c07467
ACS Omega 2024, 9, 15818−15832

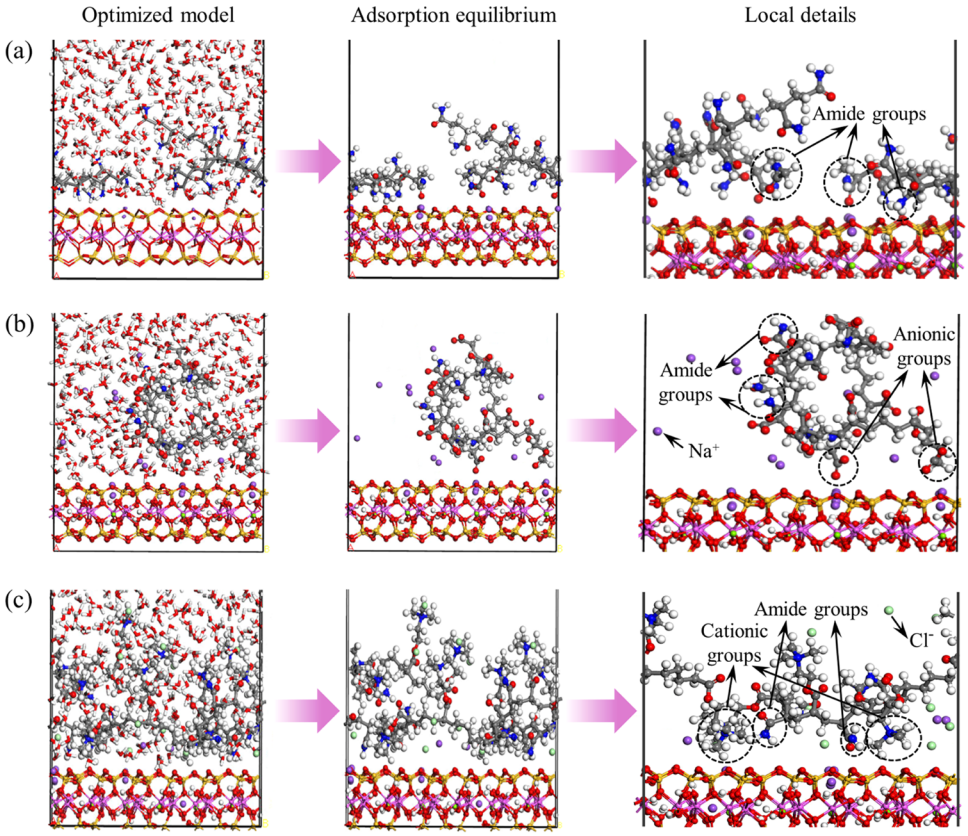

Figure 12. Equilibrium adsorption configurations of (a) NPAM, (b) APAM, and (c) CPAM on the MMT Na--001 surface.

adsorption was 18.66 to −52.99 eV, that of MMT Na-001 after NPAM adsorption was 18.57 to −52.75 eV, that of MMT Na-001 after APAM adsorption was 16.93 to −52.94 eV, and that of MMT Na-001 after CPAM adsorption was 14.22 to −56.53 eV. Therefore, after PAM adsorption, the DOS of MMT migrated to the lower energy region compared with that before adsorption, indicating that more electrons occupied the low energy state after adsorption. The orbital energy of the system decreased, so the system stability was enhanced, that is, the order of adsorption stability of the MMT Na-001 surface was CPAM > APAM > NPAM.

The DOS of the MMT None-001 surface was in the range of 18.66 to −52.90 eV before adsorption of PAM and in the range of 13.81 to −56.82 eV after CPAM adsorption. The DOS curve of MMT None-001 changed little after adsorption of NPAM, only the height decreased a little. Therefore, the order of adsorption stability of the MMT None-001 surface was CPAM > NPAM. These results correspond to the calculated results of adsorption energy.

In Section 3.6, track of the analysis showed that the activity of O atoms on the surface of MMT is mainly provided by the 2p orbital, so the PDOS of the O 2p orbital on the MMT surface before and after CPAM adsorption was analyzed; at the same time, the p-band center (ε_p) was calculated, as shown in Figure 11c,d. After CPAM adsorption, the PDOS peaks of the O 2p orbital on the MMT Na-001 surface and None-001 surface shifted to the left, and ε_p shifted to the left compared with before adsorption. Therefore, the activity of the O atom on the surface of MMT decreases and the stability of the system increases after CPAM adsorption. Therefore, we conclude that the left shift of ε_p of the O atom on the MMT surface is conducive to the stable adsorption of CPAM.

3.7. MD Calculation Results. *3.7.1. Adsorption Configuration and Energy.* The equilibrium adsorption configurations of the three PAM on the surface of the MMT Na-001 surface based on molecular dynamics calculations are shown in Figure 12. All three PAM tended to be adsorbed on the MMT Na-001 surface, and N−H···O hydrogen bonds were formed between the H atoms on the amino group of NPAM ($CONH_2$) and the oxygen atoms on the Na-001 surface. Meanwhile, the O atoms on the amino group also interacted with the Na atoms on the Na-001 surface. APAM and the MMT Na-001 surface were mainly dominated by the adsorption of anionic groups (COO^-) and Na ions, and the amino groups were far away from the surface, indicating that the interaction between anionic groups and the Na-001 surface is stronger. Both the cationic functional group ($N(CH_3)_3^+$) and amide group ($CONH_2$) of CPAM can adsorb to the surface of MMT, and the cationic functional group ($N(CH_3)_3^+$) was closer to the surface of MMT, indicating that the interaction between them is stronger. The MD results presented above were basically consistent with the DFT results. In addition, it can be seen that the counterions (Cl^- and Na^+) of CPAM and APAM were distributed near the Na-001 surface, which may be affected by the electrostatic interaction on the Na-001 surface.

To further quantify and analyze the adsorption, the interaction energy results based on molecular dynamics calculations are shown in Figure 13. When the three PAM adsorbs on the MMT Na-001 surface, the electrostatic interaction energy accounts for the main part of the adsorption energy, and the van der Waals interaction energy accounts for a small part, indicating that the main effect of their adsorption is electrostatic interaction. The total interaction energies between

https://doi.org/10.1021/acsomega.3c07467
ACS Omega 2024, 9, 15818−15832

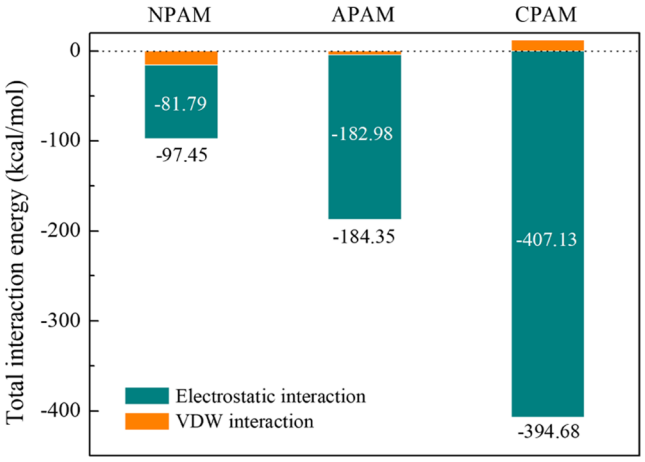

Figure 13. Surface adsorption interaction energy of three PAM with the MMT Na-001 surface.

NPAM, APAM, and CPAM and the MMT Na-001 surface were −97.45, −184.35, and −394.68 kcal/mol, respectively. At the same time, the adsorption distance and the spatial morphology of the molecule (group) preliminarily determine the strength and form of PAM adsorption on the Na-001 surface. That is, the magnitude of the interaction energy was CPAM > APAM > NPAM. This result was in the same order as the adsorption energy calculated by DFT.

3.7.2. Spatial Distribution of Water Molecules. The surface hydrophobicity of materials will be affected by the addition of chemicals.[57] By calculation of the concentration profiles of the three PAM and water molecules, the influence of water molecules on the adsorption behavior of the three PAM and the MMT Na-001 surface was analyzed from the perspective of spatial distribution, and the results are shown in Figure 14. It showed that the high-density water molecular layer of the three PAM and the MMT Na-001 surface adsorption system in aqueous solution was located at 11.14, 11.14, and 8.53 Å, respectively. Compared with the initial position of the MMT Na-001 surface (10.07, 10.07, and 6.99 Å in the three systems, respectively), the distances between the high-density water layer and the surface were 1.07, 1.07, and 1.54 Å, respectively. It indicates that CPAM tends to be farther away from the MMT Na-001 surface than NPAM and APAM.

The dense layer of water molecules on mineral surfaces is usually regarded as a hydration film.[58] In Figure 14a, the concentration of water molecules in the distance range of 15−30 Å showed a decreasing trend, because this spatial range was the aggregation area of PAM (Figure 14b). At adsorption equilibrium, the three PAM were located at 9.07, 9.07, and 6.08 Å, respectively. By comparing the results in Figure 14a, it can be seen that the three PAM were closer to the surface of MMT Na-001 than water molecules, indicating that PAM can break through the hydration film and adsorb on the MMT Na-001 surface.

Through the two-dimensional image of spatial distribution of water molecules (Figure 14c), it can be intuitively seen that the density of water molecules around PAM was low, indicating that PAM can keep water molecules away from the surface of the MMT Na-001 surface, thereby enhancing its surface hydrophobicity. Compared with NPAM and APAM, CPAM has the strongest alienating effect on water molecules on the MMT Na-001 surface.

3.7.3. Self-Diffusion Coefficient of PAM. Figure 14 shows that the three PAM can break through the hydration layer to achieve the effect of keeping water molecules away from the MMT Na-001 surface. To understand the motion characteristics of the three PAM on the MMT Na-001 surface in aqueous solution, the MSD and diffusion coefficients of the

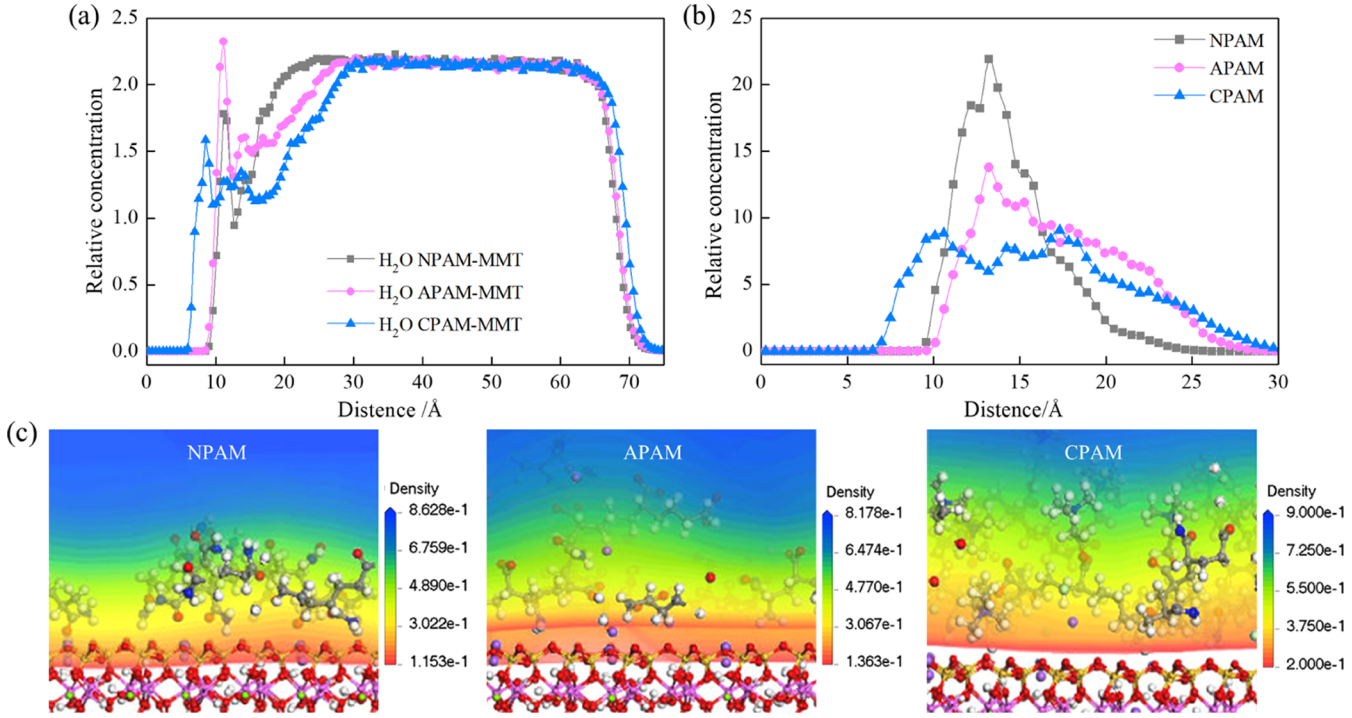

Figure 14. Density distribution of (a) three PAM and (b) water molecules in aqueous solution and the average density field of water molecules in (c) three PAM systems.

https://doi.org/10.1021/acsomega.3c07467
ACS Omega 2024, 9, 15818−15832

three PAM with respect to the MMT Na-001 surface were analyzed, and the results are shown in Figure 15. It can be seen

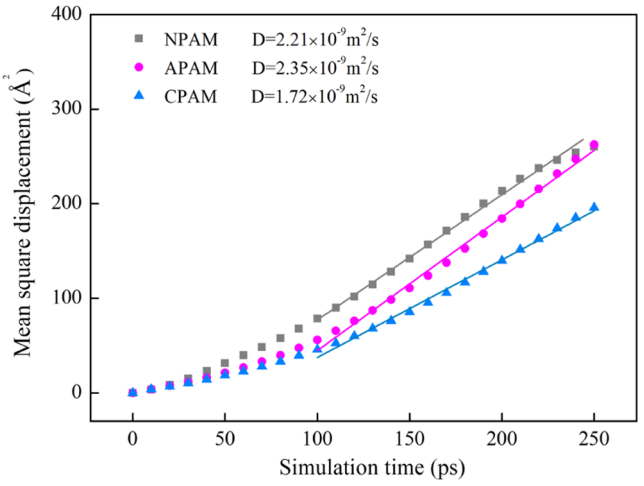

Figure 15. MSD and diffusion coefficient of three PAM on the MMT Na-001 surface.

that the diffusion coefficient D calculated by fitting the MSD results of the three PAM were 2.21 × 10^{-9} m^2/s (NPAM), 2.35 × 10^{-9} m^2/s (APAM), and 1.72 × 10^{-9} m^2/s (CPAM), respectively. The results showed that the diffusion ability of the three PAM on the surface of MMT Na-001 after adsorption equilibrium was APAM > NPAM > CPAM. This means that CPAM is most significantly bound by the MMT Na-001 surface, The results were consistent with the laws obtained from the adsorption energy and the concentration distribution.

4. CONCLUSIONS

In this study, the adsorption behaviors of three PAM on the MMT (001) surface were studied through sedimentation and filtration tests, ζ-potential, low-field NMR analysis, and DFT simulations. The adsorption differences of the three PAM were revealed. The conclusions were as follows:

The flocculation effect of the three PAMs on MMT was CPAM > NPAM > APAM, and the pressure filtration effect of coal slime water also had the same law.

ζ-potential detection showed that the main effect of NPAM and APAM flocculants in the settlement and pressure filtration of coal slime water was flocculation, while CPAM had an electric neutralization effect in addition to flocculation. After adsorption of PAM by MMT, flocculation occurs between particles, resulting in an increase of particle size and a decrease of specific surface area. The change in the specific surface area of MMT was directly related to the change in the pore characteristics. The total pore volume of MMT decreases, and the average pore size increases under PAM. LF-NMR indicated that PAM could remove the vicinal water from the surface of mineral particles through flocculation but not between MMT layers.

The order of adsorption interactions for the PAM structural elements adsorbed on the MMT Na-001 surface was CPAM > APAM > NPAM, and the order of the adsorption interactions for the PAM structural elements adsorbed on the MMT None-001 surface was CPAM > NPAM > APAM. NPAM had coordination and hydrogen bonding with the MMT Na-001 surface, NPAM had hydrogen bonding with the MMT None-001 surface, APAM had coordination with the MMT Na-001 surface, and CPAM had electrostatic coordination with the Na-001 surface. The main form of adsorption between CPAM and the None-001 surface was electrostatic. Therefore, the interaction between the three PAM structural units and MMT was nonbonding. And the left shift of ε_p of the O atom on the MMT surface was conducive to the stable adsorption of CPAM. PAM can penetrate the hydration film and adsorb onto the MMT surface, and the presence of PAM reduced the concentration of water molecules around the MMT surface. And the order of PAM diffusion on the MMT Na-001 surface was APAM > NPAM > CPAM. This means that CPAM is most significantly bound by the MMT Na-001 surface.

At present, the model size and time of all simulation calculations are limited by the computing power of the computer. The simulation results in the existing literature are calculated based on a single or a small number of pharmaceutical molecules, and they all realize the mutual verification of simulation results and experimental results as in this study. However, due to size limitations, the polymer concentration used in the simulation work is much higher than the experimental value. The above problems will be gradually improved with the development of computers.

■ ASSOCIATED CONTENT

Supporting Information

The Supporting Information is available free of charge at https://pubs.acs.org/doi/10.1021/acsomega.3c07467.

Fukui index of the three PAM structural units and Hirshfeld charge before and after adsorption of three PAM structural units on the MMT(001) surface (PDF)

■ AUTHOR INFORMATION

Corresponding Authors

Mohamed-Tahar Ammami − *Normandie University, ULHN, LOMC UMR CNRS, 6294 Le Havre, France*; Email: mohamed-tahar.ammami@univ-lehavre.fr

Lubin Wei − *School of Chemical and Environmental Engineering, China University of Mining and Technology (Beijing), Beijing 100083, P. R. China*; Email: wlb@cumtb.edu.cn

Authors

Xiaohui Yan − *School of Chemical and Environmental Engineering, China University of Mining and Technology (Beijing), Beijing 100083, P. R. China; Normandie University, ULHN, LOMC UMR CNRS, 6294 Le Havre, France*; orcid.org/0000-0002-8950-9983

Qi Meng − *School of Chemical and Environmental Engineering, China University of Mining and Technology (Beijing), Beijing 100083, P. R. China*

Complete contact information is available at: https://pubs.acs.org/10.1021/acsomega.3c07467

Author Contributions

X.Y.: Conceptualization, methodology, software, validation, investigation, writing—original draft, and writing—review and editing. Q.M.: Writing—review and editing, conceptualization, methodology, and investigation. M.A. and L.W.: Conceptualization, writing—review and editing, and supervision.

Notes

The authors declare no competing financial interest.

https://doi.org/10.1021/acsomega.3c07467
ACS Omega 2024, 9, 15818−15832

■ ACKNOWLEDGMENTS

This research did not receive any specific grant from funding agencies in the public, commercial, or not-for-profit sectors.

■ REFERENCES

(1) Sabah, E.; Cengiz, I. An evaluation procedure for flocculation of coal preparation plant tailings. *Water Res.* **2004**, *38* (6), 1542−1549.
(2) Chen, X.; Peng, Y. Managing clay minerals in froth flotation—A critical review. *Miner. Process. Extr. Metall. Rev.* **2018**, *39* (5), 289−307.
(3) Wu, Y.; Wang, C.; Xu, J. Aqueous dispersion polymerization of amphoteric polyacrylamide. *J. Appl. Polym. Sci.* **2010**, *115* (2), 1131−1137.
(4) Wang, C.; Harbottle, D.; Liu, Q.; Xu, Z. Current state of fine mineral tailings treatment: A critical review on theory and practice. *Miner. Eng.* **2014**, *58*, 113−131.
(5) Hu, Y.; Qiu, G.; Wang, D. *Interaction between Particles and Fine Flotation*; Central South University of technology press: Changsha, 1993.
(6) Liu, D.; Edraki, M.; Berry, L. Investigating the settling behaviour of saline tailing suspensions using kaolinite, bentonite, and Illite clay minerals. *Powder Technol.* **2018**, *326*, 228−236.
(7) Ofori, P.; Nguyen, A. V.; Firth, B.; McNally, C.; Ozdemir, O. Shear-induced floc structure changes for enhanced dewatering of coal preparation plant tailings. *Chem. Eng. J.* **2011**, *172* (2−3), 914−923.
(8) Chang, Z. Y.; Sun, C. B.; Kou, J.; Fu, G. Q.; Qi, X. Y. Experimental and molecular dynamics simulation study on the effect of polyacrylamide on bauxite flotation. *Miner. Eng.* **2021**, *164*, No. 106810, DOI: 10.1016/j.mineng.2021.106810.
(9) Teepakakorn, A.; Ogawa, M. Interactions of layered clay minerals with water-soluble polymers; structural design and functions. *Appl. Clay Sci.* **2022**, *222*, No. 106487.
(10) Deng, Y.; Dixon, J. B.; White, G. N. Adsorption of polyacrylamide on smectite, Illite, and kaolinite. *Soil Sci. Soc. Am. J.* **2006**, *70* (1), 297−304.
(11) Chen, Z.; Li, Y.; Chen, C.; Sun, X.; Liu, W. Aggregation Behavior of Asphalt on the Natural Gas Hydrate Surface with Different Surfactant Coverages. *J. Phys. Chem. C* **2021**, *125* (30), 16378−16390.
(12) Wiśniewska, M.; Fijałkowska, G.; Szewczuk-Karpisz, K. The mechanism of anionic polyacrylamide adsorption on the montmorillonite surface in the presence of Cr(VI) ions. *Chemosphere* **2018**, *211*, 524−534.
(13) Mpofu, P.; Addai-Mensah, J.; Ralston, J. Investigation of the effect of polymer structure type on flocculation, rheology and dewatering behaviour of kaolinite dispersions. *Int. J. Miner. Process.* **2003**, *71* (1), 247−268.
(14) Cai, M.; Qian, Z.; Xiong, X.; Dong, C.; Song, Z.; Shi, Y.; Wei, Z.; Jin, M. Cationic polyacrylamide (CPAM) enhanced pressurized vertical electro-osmotic dewatering of activated sludge. *Sci. Total Environ.* **2022**, *818*, No. 151787.
(15) Molaei, N.; Chelgani, S. C.; Bobicki, E. R. A comparison study between bioflocculants and PAM for dewatering of ultrafine phyllosilicate clay minerals. *Appl. Clay Sci.* **2022**, *218*, No. 106409.
(16) Hyrycz, M.; Ochowiak, M.; Krupińska, A.; Włodarczak, S.; Matuszak, M. A review of flocculants as an efficient method for increasing the efficiency of municipal sludge dewatering: Mechanisms, performances, influencing factors and perspectives. *Sci. Total Environ.* **2022**, *820*, No. 153328.
(17) Chen, J.; Min, F. F.; Liu, L. Y.; Liu, C. F. Mechanism research on surface hydration of kaolinite, insights from DFT and MD simulations. *Appl. Surf. Sci.* **2019**, *476*, 6−15.
(18) Chen, Z.; Sun, J.; Wu, P.; Liu, W.; Chen, C.; Lang, C.; Dai, S.; Zhou, W. Cyclodextrin as a green anti-agglomerant agent in oil−water emulsion containing asphalt. *Fuel* **2023**, *335*, No. 127041, DOI: 10.1016/j.fuel.2022.127041.
(19) Chen, Z.; Liu, W.; Sun, J.; Chen, C.; Song, Y. Alanine rich amphiphilic peptides as green substitutes for hydrate inhibitors: A molecular simulation study. *J. Mol. Liq.* **2023**, *370*, No. 121008, DOI: 10.1016/j.molliq.2022.121008.
(20) Han, Y.; Liu, W.; Chen, J. DFT simulation of the adsorption of sodium silicate species on kaolinite surfaces. *Appl. Surf. Sci.* **2016**, *370*, 403−409.
(21) Peng, C.; Min, F.; Liu, L.; Chen, J. periodic DFT study of adsorption of water on sodium-montmorillonite (001) basal and (010) edge surface. *Appl. Surf. Sci.* **2016**, *387*, 308−316.
(22) Han, Z.; Cui, Y.; Meng, Q.; He, M.; Yan, X. The effect of inorganic salt on the mechanical properties of montmorillonite and its mechanism: A molecular dynamics study. *Chem. Phys. Lett.* **2021**, *781*, No. 138982.
(23) Zhang, L.; Min, F.; Chen, J.; Liu, C.; Wang, T. New insights into the interaction between monomers from acrylamide-based polymeric flocculants and montmorillonite: A DFT study. *J. Mol. Liq.* **2022**, *365*, No. 120171.
(24) Xu, J.; Wang, X.; Chen, J.; Ding, T.; Xue, J. Inhibition mechanism of cationic polyacrylamide on montmorillonite surface hydration: A molecular dynamics simulation study. *Chem. Phys.* **2023**, *567*, No. 111792.
(25) Delley, B. DMol3 DFT studies: from molecules and molecular environments to surfaces and solids. *Comput. Mater. Sci.* **2000**, *17* (2), 122−126.
(26) Clark, S. J.; Segall, M. D.; Pickard, C. J.; Hasnip, P. J.; Probert, M. I. J.; Payne, K. R. a. M. C. First principles methods using CASTEP. *Z. Kristallogr. - Cryst. Mater.* **2005**, *220* (5−6), 567−570, DOI: 10.1524/zkri.220.5.567.65075.
(27) Segall, M. D.; Shah, R.; Pickard, C. J.; Payne, M. Population analysis of plane-wave electronic structure calculations of bulk materials. *Phys. Rev. B* **1996**, *54* (23), 16317−16320.
(28) Yang, Z.; Liu, W.; Zhang, H.; Jiang, X.; Min, F. DFT study of the adsorption of 3-chloro-2-hydroxypropyl trimethylammonium chloride on montmorillonite surfaces in solution. *Appl. Surf. Sci.* **2018**, *436*, 58−65.
(29) Shaikh, S. M. R.; Nasser, M. S.; Hussein, I.; Benamor, A.; Onaizi, S. A.; Qiblawey, H. Influence of polyelectrolytes and other polymer complexes on the flocculation and rheological behaviors of clay minerals: A comprehensive review. *Sep. Purif. Technol.* **2017**, *187*, 137−161.
(30) Zhu, J.; Zheng, H.; Jiang, Z.; Zhang, Z.; Liu, L.; Sun, Y.; Tshukudu, T. Synthesis and characterization of a dewatering reagent: cationic polyacrylamide (P(AM-MC-DA)) for activated sludge dewatering treatment. *Desalin. Water Treat.* **2013**, *51* (13−15), 2791−2801.
(31) Guan, Q.; Zhu, G.; Liao, Y.; Xu, J.; Sun, X.; Tian, F.; Xu, J.; Luo, M. Preparation, Characterization, and Sludge Conditioning of Cationic Polyacrylamide Synthesized by a Novel UVA-Initiated System. *Processes* **2018**, *6* (12), No. 233, DOI: 10.3390/pr6120233.
(32) Heyd, J.; Scuseria, G. E. Assessment and validation of a screened Coulomb hybrid density functional. *J. Chem. Phys.* **2004**, *120* (16), 7274−7280.
(33) Ireta, J.; Neugebauer, J.; Scheffler, M. On the accuracy of DFT for describing hydrogen bonds: Dependence on the bond directionality. *J. Phys. Chem. A* **2004**, *108* (26), 5692−5698.
(34) Perdew, J. P.; Burke, K.; Ernzerhof, M. Generalized Gradient Approximation Made Simple. *Phys. Rev. Lett.* **1996**, *77* (18), 3865−3868.
(35) Peng, C. *The Mechanism of Hydration and Hydrophobic Improvement of Montmorillonite in Aqueous Solutions: A Quantum Mechanics/molecular Dynamics Simulation Study*; Anhui University of Science and Technology: Huainan, 2016.
(36) Wardle, R.; Brindley, G. W. The crystal structures of pyrophyllite, 1Te, and of its dehydroxylate. *Am. Mineral.* **1972**, *57* (5−6), 732−750.
(37) Soley, M.; Markmann, A.; Batista, V. S. Steered Quantum Dynamics for Energy Minimization. *J. Phys. Chem. B* **2015**, *119* (3), 715−727.

https://doi.org/10.1021/acsomega.3c07467
ACS Omega 2024, 9, 15818−15832

(38) Amaya-Roncancio, S.; Blanco, A. A. G.; Linares, D. H.; Sapag, K. DFT study of hydrogen adsorption on Ni/graphene. *Appl. Surf. Sci.* **2018**, *447*, 254−260.
(39) Chandrasekaran, S.; Li, N.; Zhuang, Y.; Sui, L.; Xiao, Z.; Fan, D.; Aravindan, V.; Bowen, C.; Lu, H.; Liu, Y. Interface charge density modulation of a lamellar-like spatially separated Ni9S8 nanosheet/Nb2O5 nanobelt heterostructure catalyst coupled with nitrogen and metal (M = Co, Fe, or Cu) atoms to accelerate acidic and alkaline hydrogen evolution reactions. *Chem. Eng. J.* **2022**, *431*, No. 134073, DOI: 10.1016/j.cej.2021.134073.
(40) Xiong, B. Y.; Loss, R. D.; Shields, D.; Pawlik, T.; Hochreiter, R.; Zydney, A. L.; Kumar, M. Polyacrylamide degradation and its implications in environmental systems. *npj Clean Water* **2018**, *1*, No. 17, DOI: 10.1038/s41545-018-0016-8.
(41) Allen, M. P.; Tildesley, D. J. *Computer Simulation of Liquids*; Oxford Academic, 1987.
(42) Einstein, A. B. On the movement of small particles suspended in a stationary liquid demanded by the molecular-kinetic theory of heart. *Ann. Phys. 17*, 549 560.
(43) Pan, M.; Duan, C.; Huang, L.; Wang, W.; Jiang, H.; Qiao, J.; Zhao, Y. Describing the adsorption of PAM on coal/kaolinite surface in aquatic by combining experiments and MD simulation. *J. Mol. Liq.* **2023**, *372*, No. 121152.
(44) Chang, Z.; Sun, C.; Kou, J.; Fu, G.; Qi, X. Experimental and molecular dynamics simulation study on the effect of polyacrylamide on bauxite flotation. *Miner. Eng.* **2021**, *164*, No. 106810.
(45) Norrish, K. The swelling of montmorillonite. *Discuss. Faraday Soc.* **1954**, *18*, 120−134.
(46) Zou, W.; Gong, L.; Huang, J.; Pan, M.; Lu, Z.; Sun, C.; Zeng, H. Probing the adsorption and interaction mechanisms of hydrophobically modified polyacrylamide P(AM-NaAA-C16DMAAC) on model coal surface: Impact of salinity. *Miner. Eng.* **2019**, *141*, No. 105841.
(47) Shaikh, S. M.; Nasser, M. S.; Magzoub, M.; Benamor, A.; Hussein, I. A.; El-Naas, M. H.; Qiblawey, H. Effect of electrolytes on electrokinetics and flocculation behavior of bentonite-polyacrylamide dispersions. *Appl. Clay Sci.* **2018**, *158*, 46−54.
(48) Shaikh, S. M. R.; Nasser, M. S.; Hussein, I. A.; Benamor, A. Investigation of the effect of polyelectrolyte structure and type on the electrokinetics and flocculation behavior of bentonite dispersions. *Chem. Eng. J.* **2017**, *311*, 265−276.
(49) Nasser, M. S.; James, A. E. The effect of polyacrylamide charge density and molecular weight on the flocculation and sedimentation behaviour of kaolinite suspensions. *Sep. Purif. Technol.* **2006**, *52* (2), 241−252.
(50) Vesilind, P. A. The role of water in sludge dewatering. *Water Environ. Res.* **1994**, *66*, 4−11, DOI: 10.2175/WER.66.1.2.
(51) Theng, B. K. G. Clay-Polymer Interactions: Summary and Perspectives. *Clays Clay Miner.* **1982**, *30* (1), 1−10.
(52) Inyang, H. I.; Bae, S. Polyacrylamide sorption opportunity on interlayer and external pore surfaces of contaminant barrier clays. *Chemosphere* **2005**, *58* (1), 19−31.
(53) Bredas, J.-L. Mind the gap! *Mater. Horiz.* **2014**, *1* (1), 17−19.
(54) Ren, B.; Min, F.; Liu, L.; Chen, J.; Liu, C.; Lv, K. Adsorption of different PAM structural units on kaolinite (0 0 1) surface: Density functional theory study. *Appl. Surf. Sci.* **2020**, *504*, No. 144324.
(55) Lgaz, H.; Bhat, K. S.; Salghi, R.; Shubhalaxmi; Jodeh, S.; Algarra, M.; Hammouti, B.; Ali, I. H.; Essamri, A. Insights into corrosion inhibition behavior of three chalcone derivatives for mild steel in hydrochloric acid solution. *J. Mol. Liq.* **2017**, *238*, 71−83.
(56) Fukui, K.; Koga, N.; Fujimoto, H. Interaction frontier orbitals. *J. Am. Chem. Soc.* **1981**, *103* (1), 196−197.
(57) Li, H.; Yang, W.; Wu, C.; Xu, J. Origin of the hydrophobicity of sulfur-containing iron surfaces. *Phys. Chem. Chem. Phys.* **2021**, *23* (25), 13971−13976.
(58) Zhao, Y.; Yi, H.; Jia, F.; Li, H.; Peng, C.; Song, S. A novel method for determining the thickness of hydration shells on nanosheets: A case of montmorillonite in water. *Powder Technol.* **2017**, *306*, 74−79.

https://doi.org/10.1021/acsomega.3c07467
ACS Omega 2024, 9, 15818−15832